Endothelial PHD2 deficiency induces nitrative stress *via* suppression of caveolin-1 in pulmonary hypertension

Bin Liu[1,2], Yi Peng[3,4,5], Dan Yi[1,2], Narsa Machireddy[3,4,5], Daoyin Dong[3,4,5], Karina Ramirez[1,2], Jingbo Dai[3,4,5], Rebecca Vanderpool[6], Maggie M. Zhu[3,4,5], Zhiyu Dai[1,2,10] and You-Yang Zhao[3,4,5,7,8,9,10]

[1]Division of Pulmonary, Critical Care and Sleep, Dept of Internal Medicine, University of Arizona, Phoenix, AZ, USA. [2]Translational Cardiovascular Research Center, College of Medicine-Phoenix, University of Arizona, Phoenix, AZ, USA. [3]Program for Lung and Vascular Biology, Ann and Robert H. Lurie Children's Hospital of Chicago, Chicago, IL, USA. [4]Section for Injury Repair and Regeneration Research, Stanley Manne Children's Research Institute, Ann and Robert H. Lurie Children's Hospital of Chicago, Chicago, IL, USA. [5]Division of Critical Care, Dept of Pediatrics, Northwestern University Feinberg School of Medicine, Chicago, IL, USA. [6]College of Medicine Division of Cardiovascular Medicine, The Ohio State University, Columbus, OH, USA. [7]Dept of Pharmacology, Northwestern University Feinberg School of Medicine, Chicago, IL, USA. [8]Dept of Medicine, Northwestern University Feinberg School of Medicine, Chicago, IL, USA. [9]Feinberg Cardiovascular and Renal Research Institute, Northwestern University Feinberg School of Medicine, Chicago, IL, USA. [10]Zhiyu Dai and You-Yang Zhao contributed equally to this article as lead authors and supervised the work.

Corresponding author: You-Yang Zhao (Youyang.zhao@northwestern.edu)

Shareable abstract (@ERSpublications)
Endothelial PHD2 deficiency decreases caveolin-1 expression leading to augmented nitrative stress, which contributes to obliterative pulmonary vascular remodelling and severe pulmonary hypertension https://bit.ly/3yw48zm

Cite this article as: Liu B, Peng Y, Yi D, *et al*. Endothelial PHD2 deficiency induces nitrative stress *via* suppression of caveolin-1 in pulmonary hypertension. *Eur Respir J* 2022; 60: 2102643 [DOI: 10.1183/13993003.02643-2021].

This article has an editorial commentary: https://doi.org/10.1183/13993003.01776-2022

Received: 19 April 2020
Accepted: 24 June 2022

Abstract

Background Nitrative stress is a characteristic feature of the pathology of human pulmonary arterial hypertension. However, the role of nitrative stress in the pathogenesis of obliterative vascular remodelling and severe pulmonary arterial hypertension remains largely unclear.

Method Our recently identified novel mouse model (*Egln1*^{Tie2Cre}, *Egln1* encoding prolyl hydroxylase 2 (PHD2)) has obliterative vascular remodelling and right heart failure, making it an excellent model to use in this study to examine the role of nitrative stress in obliterative vascular remodelling.

Results Nitrative stress was markedly elevated whereas endothelial caveolin-1 (Cav1) expression was suppressed in the lungs of *Egln1*^{Tie2Cre} mice. Treatment with a superoxide dismutase mimetic, manganese (III) tetrakis (1-methyl-4-pyridyl) porphyrin pentachloride or endothelial *Nos3* knockdown using endothelial cell-targeted nanoparticle delivery of CRISPR–Cas9/guide RNA plasmid DNA inhibited obliterative pulmonary vascular remodelling and attenuated severe pulmonary hypertension in *Egln1*^{Tie2Cre} mice. Genetic restoration of Cav1 expression in *Egln1*^{Tie2Cre} mice normalised nitrative stress, reduced pulmonary hypertension and improved right heart function.

Conclusion These data suggest that suppression of Cav1 expression secondary to PHD2 deficiency augments nitrative stress through endothelial nitric oxide synthase activation, which contributes to obliterative vascular remodelling and severe pulmonary hypertension. Thus, a reactive oxygen/nitrogen species scavenger might have therapeutic potential for the inhibition of obliterative vascular remodelling and severe pulmonary arterial hypertension.

Introduction

Pulmonary arterial hypertension (PAH) is a devastating disease characterised by persistent increase of pulmonary vascular resistance and obstructive pulmonary vascular remodelling, which lead to right-sided heart failure and premature death [1–3]. Histopathological features of PAH from different aetiologies include increased vessel wall thickness, vascular fibrosis, augmented oxidative/nitrative stress, microvascular occlusion and complex plexiform lesions [4, 5]. Given that the molecular mechanisms of obliterative pulmonary vascular remodelling are not fully understood, current PAH therapies that mainly

target vasoconstriction, with little effect on vascular remodelling, are not effective in curing the disease and promoting survival [6, 7].

There is accumulating evidence of oxidative and/or nitrative stress in the lungs of patients with idiopathic PAH (IPAH). Xanthine oxidase activity involved in the generation of superoxide anions (reactive oxygen species (ROS)) is markedly increased in IPAH lungs [8], and they contribute to chronic hypoxia-induced pulmonary hypertension (PH) [9]. NADPH oxidases, including Nox1, Nox2 and Nox4, which also produce high levels of ROS, are also involved in the development of PH [10]. Staining by 8-hydroxyguanosine (a biomarker of oxidative damage caused by the reaction of superoxide with guanine) is prominent in endothelial cells (ECs) within the plexiform lesions of IPAH patients [11]. By contrast, the activity of antioxidants such as manganese superoxide dismutase (MnSOD), a key mitochondrial antioxidant enzyme coded by the *SOD2* gene, was lower in IPAH lungs [11, 12]. Excessive production of nitric oxide (NO) and superoxide leads to formation of the damaging reactive nitrogen species (RNS) peroxynitrite [13, 14]. Elevated levels of peroxynitrite (*i.e.* nitrative stress) are detrimental, and can induce cell damage and death of pulmonary vascular cells, including ECs and smooth muscle cells (SMCs) [10, 15]. In addition, peroxynitrite modifies tyrosine residue, resulting in tyrosine nitration of proteins (formation of 3-nitrotyrosine) and thus modification of their functions [13, 14, 16]. Peroxynitrite levels are elevated in the lungs of IPAH patients [11, 12], in part due to tissue hypoxia and inflammation [15]. Immunohistochemical staining shows ubiquitous 3-nitrotyrosine and a marked increase in its levels [11]. Our previous studies showed that caveolin-1 (Cav1) deficiency results in endothelial nitric oxide synthase (eNOS) activation and a marked increase in NO levels, as well as augmented production of superoxide, which form peroxynitrite leading to prominent nitrative stress in pulmonary vasculature [16, 17]. The resultant augmentation of nitrative stress causes protein kinase G (PKG) tyrosine nitration, which impairs its kinase activity, leading to enhanced vasoconstriction and vascular remodelling and thus PH as seen in $Prkg1^{-/-}$ mice (*Prkg* encodes PKG) [16, 18, 19]. PKG tyrosine nitration is markedly increased in the lungs of IPAH patients [16].

We recently reported a new mouse model of severe PH (*Tie2Cre*-mediated disruption of *Egln1*, encoding hypoxia-inducible factor (HIF) prolyl hydroxylase 2 (PHD2), designated as $Egln1^{Tie2Cre}$ (CKO)) with progressive obliterative vascular remodelling including vascular occlusion, plexiform-like lesions and right heart failure, which recapitulates many features of clinical PAH including IPAH [20, 21]. However, it is unknown whether oxidative/nitrative stress is also augmented and involved in the pathogenesis of PH in this severe PH model. In the present study, we for the first time demonstrate that endothelial PHD2 deficiency induces extensive oxidative/nitrative stress *via* downregulation of endothelial Cav1 expression in a HIF-2α-dependent manner. ROS scavenger treatment, genetic disruption of EC-specific *Nos3* or restoration of Cav1 expression markedly decreased nitrative stress and attenuated PH in CKO mice.

Methods

Animal models

All the mice used in this study are C57BL/6J background. $Egln1^{Tie2Cre}$ (CKO) and $Hif2a/Egln1^{Tie2Cre}$ (EH2) mice were generated as described previously [20]. $Cav1^{Tg}$ mice were obtained from Dr William Sessa's laboratory (Yale University, New Haven, CT, USA) [22, 23]. CKO mice were bred with $Cav1^{Tg}$ mice to generate $Egln1^{Tie2Cre}/Cav1^{Tg}$ (CKO/Tg) and $Egln1^{f/f}/Cav1^{Tg}$ (Tg) mice. Male and female $Egln1^{f/f}$ (designated as wild type (WT)), CKO, CKO/Tg and Tg littermates at age 5 weeks to 3.5 months were used in these studies. For ROS scavenger treatment, male and female CKO mice at age 5 weeks were treated with manganese (III) tetrakis (1-methyl-4-pyridyl) porphyrin pentachloride (MnTMPyP) (5 $mg \cdot kg^{-1}$) [16] intraperitoneally daily for 9 weeks. PBS was used as a control. The same PBS group was used in our previous publication [24]. The animal care and study protocols were reviewed and approved by the Institutional Animal Care and Use Committees of Northwestern University Feinberg School of Medicine, and the University of Arizona.

Echocardiography

Echocardiography was performed in the Core facilities at Northwestern University Feinberg School of Medicine and the University of Arizona as described previously [20, 25, 26]. Transthoracic echocardiography was performed on a VisualSonics Vevo 2100 or 3100 ultrasound machine (FujiFilm VisualSonics Inc.) using an MS550D (40 MHz) transducer. Right ventricle (RV) wall thickness during diastole was obtained from the parasternal short axis view at the papillary muscle level using M-mode. The RV cross-sectional area was obtained from the parasternal short axis view at the papillary muscle level using B-mode. Pulmonary artery (PA) acceleration time and PA ejection time were obtained from the parasternal short axis view at the aortic valve level using pulsed Doppler mode. Left ventricular (LV)

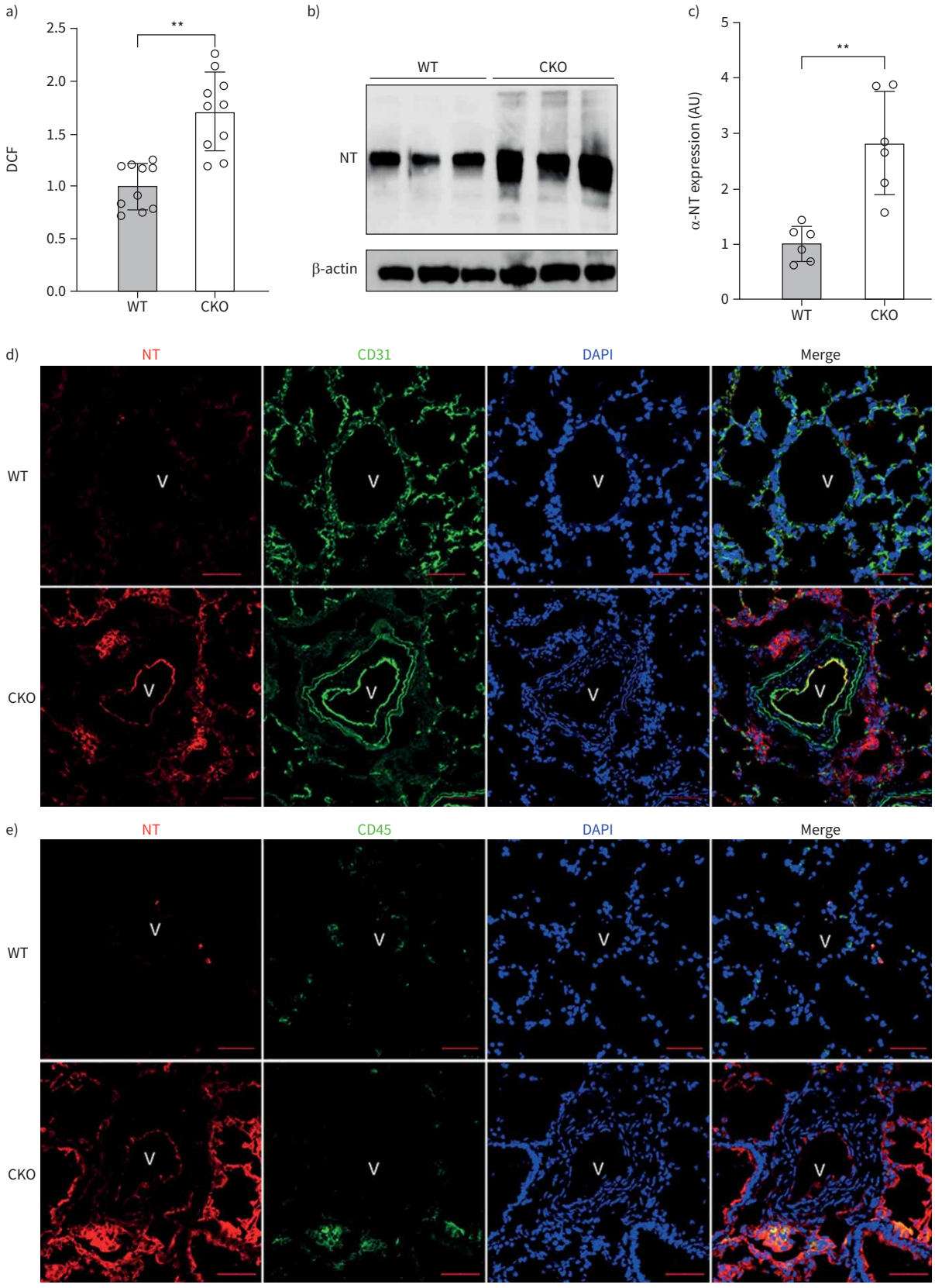

FIGURE 1 Augmented nitrative stress in pulmonary vascular lesions in *Egln1*^{Tie2Cre} (CKO) mice. a) 2′, 7′-dichlorodihydrofluorescein (DCF) measurement demonstrating marked increase of reactive oxygen species (ROS)/reactive nitrogen species (RNS) in the lungs of CKO mice. Lung tissue was collected from 3.5-month-old wild type (WT) and CKO mice for DCF assay. b, c) Western blotting demonstrating increase of nitrotyrosine

(NT) modification of proteins in the lung of CKO mice using anti-NT antibody. Anti-β-actin was used as a control. d, e) Representative micrographs of immunostaining showing prominent nitrative stress in pulmonary vascular lesions in CKO mice. Lung sections were immunostained with anti-NT antibody (red) for detection of nitrative stress. Anti-CD31 antibodies were used to label vascular endothelial cells (green, d). Anti-CD45 antibodies were used to label inflammatory cells (green, e). Nuclei were counterstained with DAPI (blue). Scale bars: 50 µm. Statistical significance for a and c determined by t-test. V: vessel. **: p<0.01.

fractional shortening and the cardiac output were obtained from the parasternal short axis view using M-mode.

Haemodynamic measurements

To measure right ventricular systolic pressure (RVSP), mice were anaesthetised with a ketamine/xylazine cocktail. A 1.4 F pressure transducer catheter (Millar Instruments) was inserted through the right jugular vein into the RV. RVSP was recorded and analysed by AcqKnowledge software (Biopac Systems Inc.) as described previously [20, 25, 26].

EC isolation

Mouse lung tissues were well perfused with PBS to remove blood. The tissues were then minced and incubated with collagenase A (1.0 $mg \cdot mL^{-1}$ in HBSS, Roche) in a shaking water bath at 37°C for 45 min, and then were dispersed by gentleMACS Dissociator (Miltenyi Biotec), followed by filtering through a 40 µm cell strainer. Cells were then incubated with anti-mouse CD31 antibody (BD Biosciences, Cat#550274, 1.5 $\mu g \cdot mL^{-1}$) on ice for 1 h, followed by incubation with sheep anti-rat IgG Dynabeads M-450 (Invitrogen, Cat#11035, 50 µL) for 30 min. Bead-bound ECs ($CD31^+$ cells) were pulled down by magnetism and lysed for protein isolation [25, 26].

Histological assessment

Mouse lung tissues were perfused with PBS, fixed with 10% formalin *via* tracheal instillation at a constant pressure (15 cmH_2O) and embedded in paraffin wax. Lung sections were stained with a Russell–Movat pentachrome staining kit (American MasterTech) according to the manufacturer's protocols. For assessment of PA wall thickness, PAs from 40 images at ×20 magnification were quantified by Image J. Wall thickness was calculated by the distance between the internal wall and external wall divided by the distance between the external wall and centre of the lumen [20, 25, 26].

Immunofluorescent staining

Mouse lung tissues were perfused with PBS, inflated with 50% optimal cutting temperature (OCT) compound in PBS and embedded in OCT for cryosectioning. For immunofluorescent staining of Cav1 and α-nitrotyrosine (NT) [16], lung sections (5 µm) were fixed with 4% paraformaldehyde and blocked with 0.1% Triton X-100 and 5% normal goat serum at room temperature for 1 h. After three washes with PBS, the slides were incubated with anti-Cav1 (Santa Cruz Biotechnology, Cat#sc-894, 1:100), anti-NT (Millipore, Cat#05-233,1:300), anti-CD31 antibody (BD Bioscience, Cat#550274, 1:25), anti-α-smooth muscle actin (α-SMA) (Abcam, Cat#Ab5694, 1:300), anti-CD45 (BioLegend, Cat#103101, 1:100) or anti-periostin (Abcam, Cat#14041, 1:100) at 4°C overnight then incubated with Alexa 594-conjugated anti-mouse IgG, Alexa 488-conjugated or 647-conjugated anti-rat or anti-rabbit IgG (Life Technology) at room temperature for 1 h. Nuclei were counterstained with DAPI contained in Prolong Gold mounting media (Life Technology).

Lung sections from formalin-fixed mouse samples were de-waxed and dehydrated, followed by boiling in 10 $mmol \cdot L^{-1}$ sodium citrate (pH 6.0) for 10 min for antigen retrieval. Slides were incubated with anti-α-SMA (Abcam, Cat#ab5694, 1:300) at 4°C overnight followed by Alexa 594-conjugated or 488-conjugated anti-rabbit IgG at room temperature for 1 h. Nuclei were counterstained with DAPI. Images were taken using the Zeiss Confocal microscope LSM880 and tiled scanning at ×20 magnification. $\alpha\text{-}SMA^+$ vessels were quantified in 40 fields per lung [20, 25, 26].

RNA isolation and quantitative reverse transcriptase PCR analysis

One lobe of lung tissue was homogenised by a TissueLyser (Qiagen) in Trizol solution (Life Technology). RNA was isolated by phenol:chloroform, followed by clean-up with Qiagen RNeasy mini kit (Qiagen). A high-capacity cDNA reverse transcription kit (Applied Biosystems) was used to transcribe 1 µg of RNA into cDNA. Quantitative reverse transcriptase PCR (RT-PCR) analysis was performed on an ABI ViiA 7 Real-Time PCR System (Applied Biosystems) with the FastStart SYBR Green Master kit (Roche Applied Science). Target mRNA expression was determined using the comparative cycle threshold method of

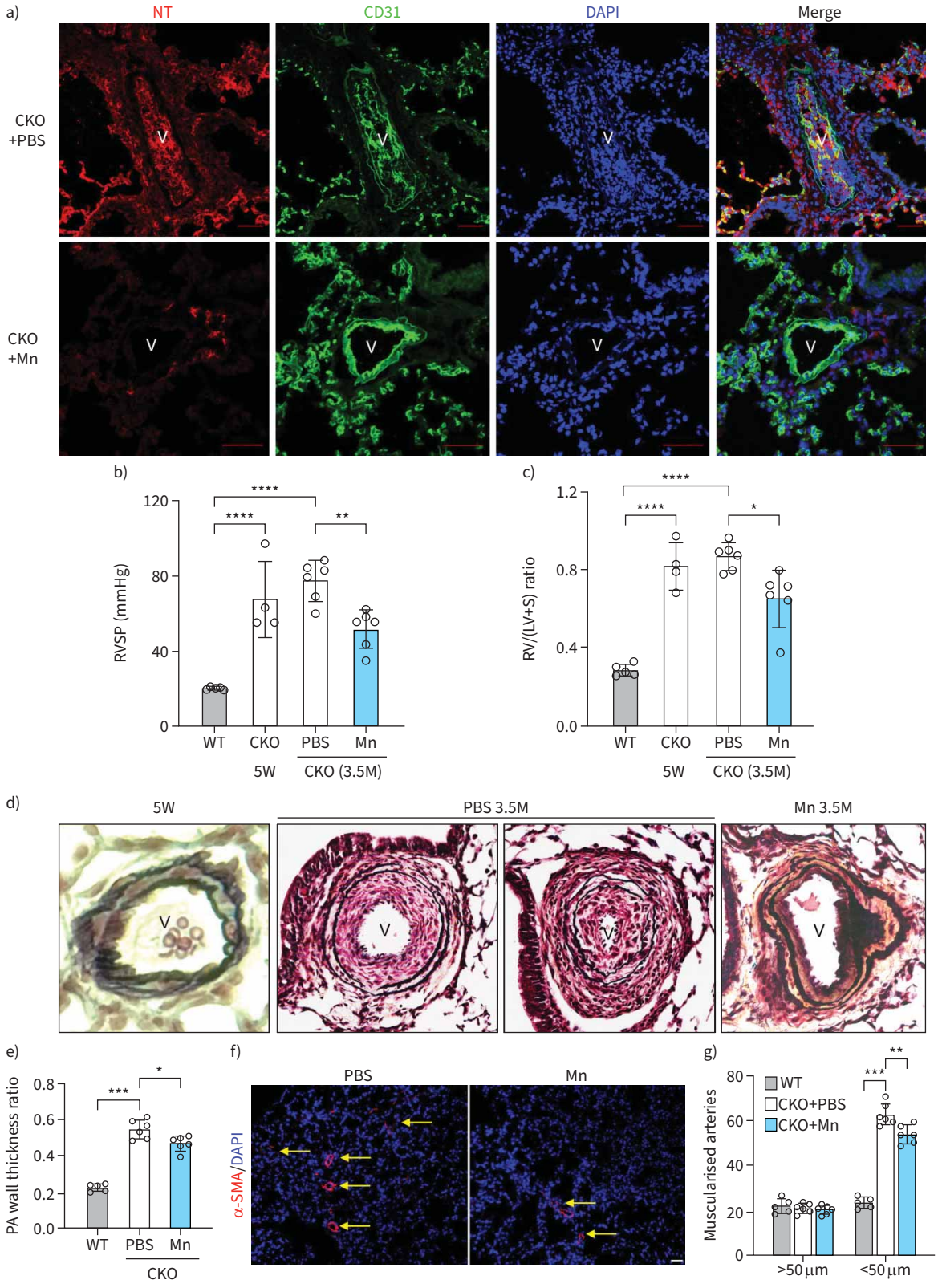

FIGURE 2 MnTMPyP (Mn) treatment reduced pulmonary hypertension in *Egln1*^{Tie2Cre} (CKO) mice. a) Immunostaining against nitrotyrosine (NT) showed that Mn treatment reduced NT modification in CKO lungs. CKO mice aged 5 weeks were treated with either Mn or PBS for 9 weeks. Scale bars: 50 μm. b, c) Right ventricular systolic pressure (RVSP) was measured and right ventricular (RV) hypertrophy determined in 3.5-month-old CKO mice (3.5M) after 9 weeks of treatment with Mn or PBS. *Egln1*$^{f/f}$ (wild type (WT)) mice were used as controls. RVSP and RV hypertrophy were also

determined in 5-week-old CKO mice (5W) without treatment. d, e) Mn treatment inhibited neointima formation and decreased pulmonary artery (PA) wall thickness. Lung sections were processed for Russell–Movat pentachrome staining. f, g) Quantification of α-smooth muscle actin (α-SMA) immunostaining demonstrated decreased muscularisation of distal pulmonary vessels in Mn-treated CKO mice. Lung cryosections were immunostained with anti-α-SMA (red) and counterstained with DAPI (blue). Arrows point to muscularised distal pulmonary vessels. Statistical significance in b, c, e and g determined by one-way ANOVA with Tukey *post hoc* analysis. V: vessel. *: p<0.05; **: p<0.01; ***: p<0.001; ****: p<0.0001.

relative quantitation. Cyclophilin A was used as an internal control. Information for mouse Cav1 and cyclophilin A primers has been described previously [20]; mouse Nos3 primers were 5′-AGGCAATCTTC GTTCAGCCA-3′ and 5′-TAGCCCGCATAGCGTATCAG-3′.

Immunoprecipitation and Western blotting

Lung tissues were collected from 3.5-month-old mice for homogenisation. 500 µg of lysates per mouse were then immunoprecipitated with anti-PKG antibody [16] and protein conjugated-Sepharose beads and blotted with anti-NT antibody (Millipore, Cat#05-233, 1:2000). The same membrane was also blotted with anti-PKG antibody (Cell Signaling Technology, Cat#13511S, 1:1000) as a loading control. Other Western blotting assays were performed using anti-Cav1 (Santa Cruz Biotechnology, Cat#sc-894 or sc-53564, 1:2000), anti-NT (Millipore, Cat#05-233, 1:2000) or anti-eNOS (BD Biosciences, Cat#610297, 1:1000). Anti-β-actin (Sigma, Cat#A2228, 1:10 000) was used as a loading control.

Measurement of ROS/RNS levels

Lung tissues were perfused free of blood with PBS, followed by collection of the left lobe. 50 mg of lung tissue was homogenised in PBS on ice. Tissue homogenates were spun at 10 000*g* for 5 min in 4°C. 50 µL of homogenates were then used for determination of tissue ROS/RNS levels (OxiSelect In Vitro ROS/RNS Assay Kit, Cat#STA-347-T) according to the manufacturer's guide. 2′, 7′-dichlorodihydrofluorescein (DCF) in the samples was measured fluorometrically against DCF standards on a fluorescence plate reader (TECAN Infinite 200 Pro). The free radical content in homogenates was determined based on the DCF standard curve. The relative DCF values were normalised by the mean value of the WT group.

Nanoparticle delivery of CRISPR plasmid DNA for EC-targeted knockdown of Nos3 *in adult mice*

To induce genome editing and knockdown of *Nos3* in ECs, plasmid DNA expressing CRISPR–Cas9 under the control of the *CDH5* promoter and two mouse *Nos3*-specific guide RNAs (gRNAs) driven by the *U6* promoter was delivered to *Egln1*^{Tie2Cre} mice by poly(lactic-co-glycolic acid) (PLGA)-based nanoparticles (Mountview Therapeutics LLC) as described previously [27]. Briefly, two gRNA sequences downstream of the start codon ATG of the *Nos3* gene encoding the 1/3 N-terminus of eNOS were designed manually (Genscript program failed to identify potent gRNAs at this region), and the single complementary DNA oligonucleotides corresponding to the gRNA sequences were commercially synthesised (Integrated DNA Technologies). The oligonucleotides were then phosphorylated, annealed and cloned sequentially into plasmid p*Sp*Cas9-2U6-GFP containing two *U6* promoters. Positive clones were confirmed by DNA sequencing. For EC-specific genomic editing, the *CAG* promoter was replaced with the human *CDH5* promoter (CRISPR^{CDH5}). The DNA sequences corresponding to the gRNAs of mouse *Nos3* were 5′-TCAGCCTATTGGCTGACGAG-3′ (reverse oligonucleotide 5′-CTCGTCAGCCAATAGGCTGA-3′) and 5′-GGATCTG ATTGCTTCAGTCA-3′ (reverse oligonucleotide 5′-TGACTGAAGCAATCAGATCC-3′).

To deliver the CRISPR^{CDH5} plasmid DNA into adult mice following the manufacturer's instruction, PLGA-based nanoparticles were mixed with plasmid DNA and incubated at room temperature for 10 min. The mixture was then administered retro-orbitally to CKO mice at 7 weeks of age (25 µg plasmid DNA per mouse) and again at 8 and 9 weeks of age (total three injections because these gRNAs are not potent). A mixture of nanoparticles:control plasmid DNA expressing a random RNA oligonucleotide was administered as a control to a separate cohort of mice. Mice were then housed until the age of 3.5 months for haemodynamic measurement and tissue collection.

Determination of genome editing efficiency in mouse lung ECs

Freshly isolated ECs from mouse lungs were digested with proteinase K overnight. The supernatants were collected after centrifugation at 20 000*g* for 10 min and extracted with a phenol:chloroform mixture followed by ethanol precipitation to isolate genomic DNA. SYBR Green-based quantitative PCR analysis of genomic DNA was carried out with the Quant Studio 6-Flex Real-Time PCR system (Applied Biosystem; SYBR Green from Roche Applied Science) to determine genome indel efficiency as described previously [27]. The sequences of the forward and reverse primers were 5′-CACGTACTCAGAGAGC CTCAA-3′ and

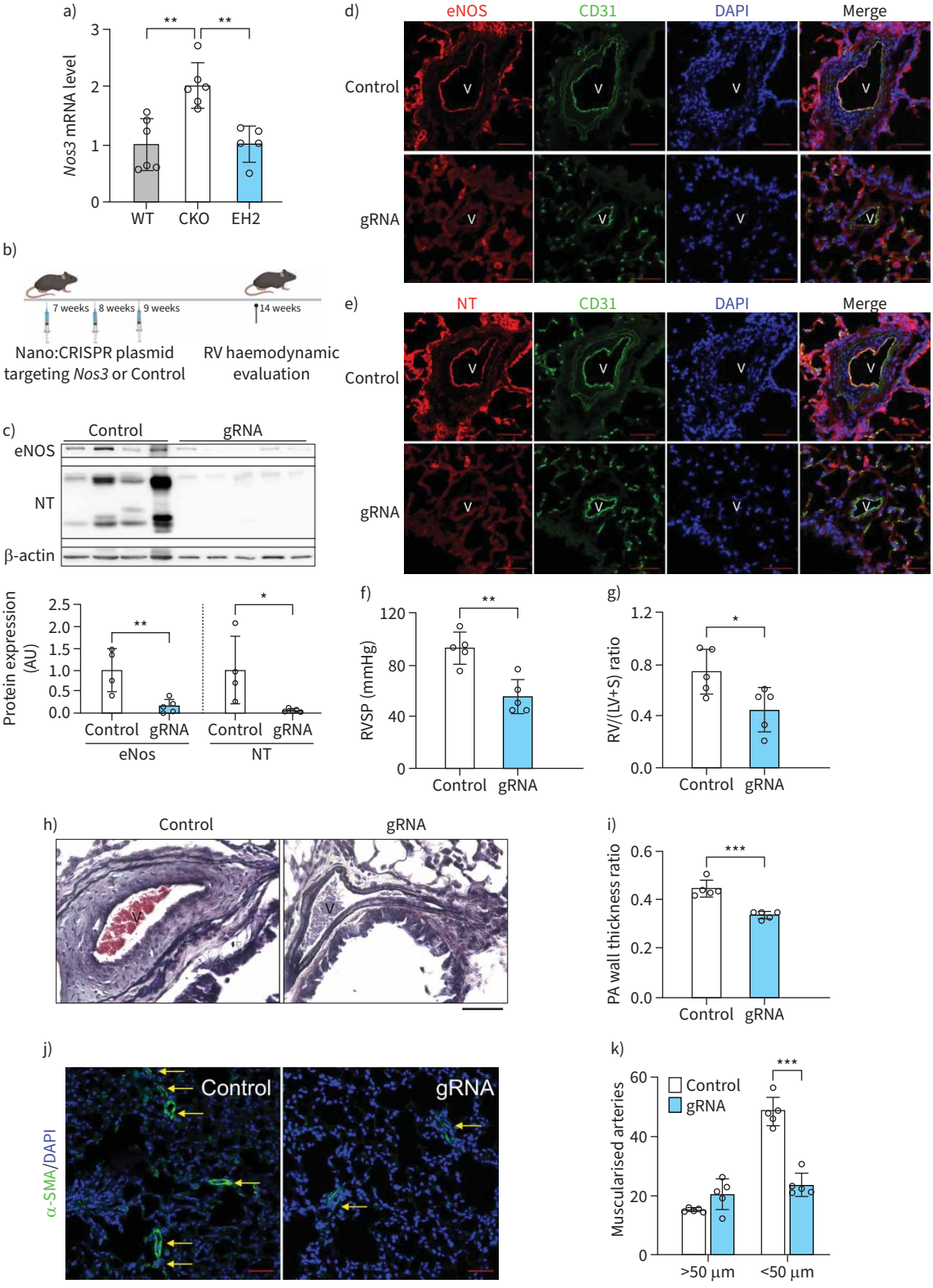

FIGURE 3 Endothelial *Nos3* knockdown attenuated pulmonary hypertension in *Egln1*^{Tie2Cre} (CKO) mice. a) Quantitative reverse transcriptase PCR analysis demonstrating *Nos3* mRNA expression is upregulated in CKO mouse lungs compared to wild type (WT) lungs and restored in *Egln1*^{Tie2Cre}/*Hif2a*^{Tie2Cre} (EH2) lungs. Lung tissue was collected from 3.5-month-old mice. b) Strategy for knockdown of endothelial *Nos3* in CKO mice. A mixture of nanoparticles:CRISPR plasmid DNA was administered to CKO mice at age 7, 8 and 9 weeks to disrupt *Nos3* expression in endothelial cells (ECs). c) Endothelial nitric oxide synthase (eNOS) protein and nitrotyrosine (NT) levels were markedly reduced in *Nos3* guide RNA (gRNA) plasmid

DNA-treated CKO mice compared with control vector DNA-treated mice. d) Immunostaining against eNOS demonstrated that eNOS was reduced in the lung ECs of *Nos3* gRNA plasmid DNA-treated CKO mice. Scale bars: 50 μm. e) Endothelial *Nos3* knockdown attenuated NT levels in the lung ECs of CKO mice. Scale bars: 50 μm. f) Haemodynamic measurement showing that endothelial *Nos3* knockdown attenuated right ventricular systolic pressure (RVSP) in CKO mice. g) Right ventricular hypertrophy (weight ratio of right ventricle/left ventricle plus septum (RV/(LV+S)) was reduced in endothelial *Nos3* knockdown CKO mice. h, i) Endothelial *Nos3* knockdown in CKO mice reduced neointima formation and decreased pulmonary artery (PA) wall thickness. Lung sections were processed for Russell–Movat pentachrome staining. Scale bars: 50 μm. j, k) Quantification of α-smooth muscle actin (α-SMA) immunostaining demonstrated decreased muscularisation of distal pulmonary vessels in endothelial *Nos3* knockdown CKO mice. Lung cryosections were immunostained with anti-α-SMA (red) and counterstained with DAPI (blue). Arrows point to muscularised distal pulmonary vessels. Scale bars: 50 μm. Statistical significance in c, d, f and h determined by one-way ANOVA with Tukey *post hoc* analysis. V: vessel. *: p<0.05, **: p<0.01; ***: p<0.001; ****: p<0.0001.

5′-AATCCTCAGCCTATTGGCTGAC-3′. The primer sequences of the control *Nme1* DNA were 5′-CCCC TTCTTTACTGGCCTGG-3′ and 5′-GCTATCCCACCAGCCTGTTT-3′ for normalisation.

Statistical analysis

Statistical significance was determined by one-way ANOVA with a Tukey *post hoc* analysis that calculates p-values corrected for multiple comparisons. Two-group comparisons were analysed by unpaired two-tailed t-test. $p<0.05$ denoted the presence of a statistically significant difference. The data in all bar graphs is presented as mean±SD.

Results

Prominent nitrative stress in Egln1^{Tie2Cre} *mouse lungs and pulmonary vascular ECs*

Given that nitrative stress is a characteristic feature of the pathology of clinical PAH, we tested whether nitrative stress is also prominent in the lung of *Egln1*^{Tie2Cre} (CKO) mice. Quantification of total free radical levels with the OxiSelect In Vitro ROS/RNS Assay Kit of lung homogenates showed that CKO lungs exhibited markedly elevated ROS/RNS levels (figure 1a). Western blotting demonstrated markedly increased levels of NT, indicative of nitrative stress, in CKO mouse lungs (figure 1b, c). We then performed NT immunostaining together with markers for ECs (CD31), inflammatory cells (CD45), fibroblasts (periostin) and SMCs (α-SMA) to determine which cell types were the NT^{+} cells in the CKO lungs. Our data showed that NT was highly expressed in the pulmonary vascular ECs and CD45^{+} inflammatory cells, with relatively low expression in pulmonary vascular SMCs and periostin^{+} fibroblasts (figure 1d, e and supplementary figure S1a, b). Our previous studies demonstrated that nitration-dependent impairment of PKG activity is involved in PH development [16]. To further determine whether PHD2 deficiency also affects PKG nitration, we performed an immunoprecipitation assay using anti-PKG antibody and blotted with anti-NT antibody. The data showed that PKG nitration was markedly increased in the lungs of CKO mice (supplementary figure S2). Together, these data demonstrate that nitrative stress is markedly augmented in the pulmonary vascular lesions in CKO mice.

ROS scavenger treatment inhibited obliterative vascular remodelling and attenuated PH in Egln1^{Tie2Cre} *mice*

We next determined whether depletion of ROS/RNS in CKO mice affected PH development. 5-week-old CKO mice with an established PH phenotype were treated intraperitoneally with the ROS/peroxynitrite scavenger MnTMPyP, which disrupts superoxide and thus peroxynitrite formation [16, 28], for 9 weeks. MnTMPyP treatment markedly reduced the levels of NT in the pulmonary vasculatures and lungs of CKO mice (figure 2a). Haemodynamic measurements showed that RVSP was reduced to ∼50 mmHg in MnTMPyP-treated CKO mice compared to ∼77 mmHg in PBS-treated CKO mice (figure 2b). RV hypertrophy, determined by the weight ratio of the RV *versus* left ventricle plus septum (LV+S), was also attenuated in MnTMPyP-treated CKO mice (figure 2c). An examination of lung pathology also revealed inhibition of occlusive vascular remodelling, evidenced by diminished neointima formation (figure 2d), and decreased PA wall thickness and muscularisation of distal pulmonary vessels in MnTMPyP-treated CKO mice compared to PBS-treated mice (figure 2e–g). Together, these data suggest the involvement of oxidative/nitrative stress in the development of severe PH in CKO mice.

Nos3 *knockdown in ECs reduced nitrative stress, vascular remodelling and severe PH in* Egln1^{Tie2Cre} *mice*

Peroxynitrite is formed by a reaction between NO and superoxide. To determine whether NO mediates nitrative stress and PH development in CKO mice, we treated CKO mice with a pan-inhibitor (N^{G}-nitro-L-arginine methyl ester (L-NAME)) of NO synthases in the drinking water (1 mg·mL^{-1}); however, all seven CKO mice died within 1 week (data not shown), suggesting that NO bioavailability is

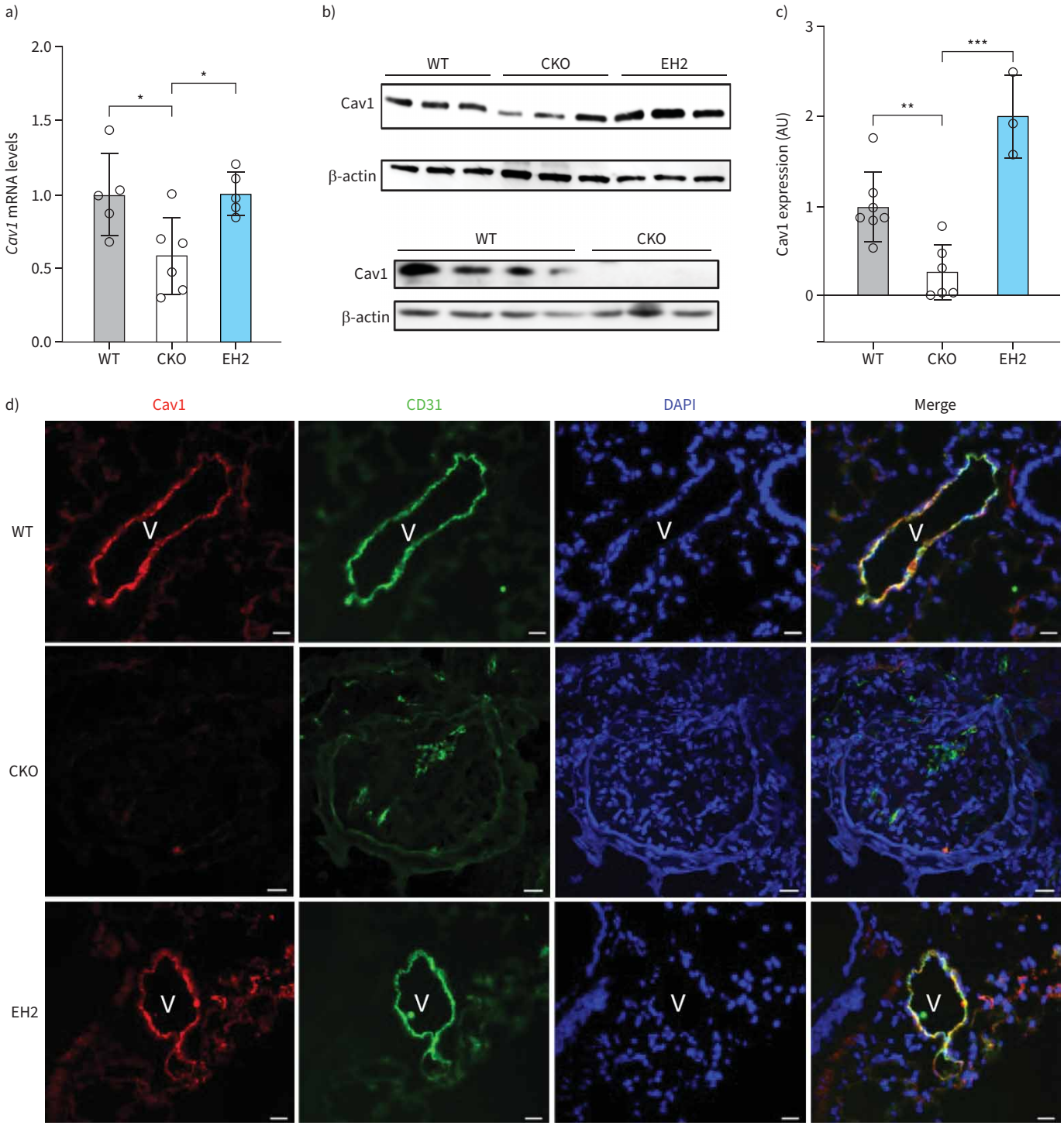

FIGURE 4 Endothelial caveolin 1 (Cav1) expression was suppressed in *Egln1*^{Tie2Cre} (CKO) mouse lungs in a hypoxia-inducible factor 2α (HIF-2α)-dependent manner. a) Quantitative reverse transcriptase PCR analysis demonstrated decreased *Cav1* mRNA expression in CKO mouse lungs compared to wild type (WT) lungs, which was restored in *Egln1*^{Tie2Cre}/*Hif2a*^{Tie2Cre} (EH2) lungs. Lung tissue was collected from 3.5-month-old mice. b, c) There was decreased Cav1 protein expression in CKO mouse lungs compared to WT lungs. Cav1 protein expression in EH2 mouse lungs was markedly increased compared to WT and CKO mouse lungs. d) Immunostaining demonstrated diminished Cav1 expression in pulmonary vascular endothelial cells of CKO mice and restoration in EH2 mice. Lung sections were immunostained with anti-Cav1 (red) and CD31 (green). Nuclei were counterstained with DAPI (blue). Scale bars: 50 μm. Statistical significance for a and c determined by one-way ANOVA with Tukey *post hoc* analysis. V: vessel. *: p<0.05; **: p<0.01; ***: p<0.001.

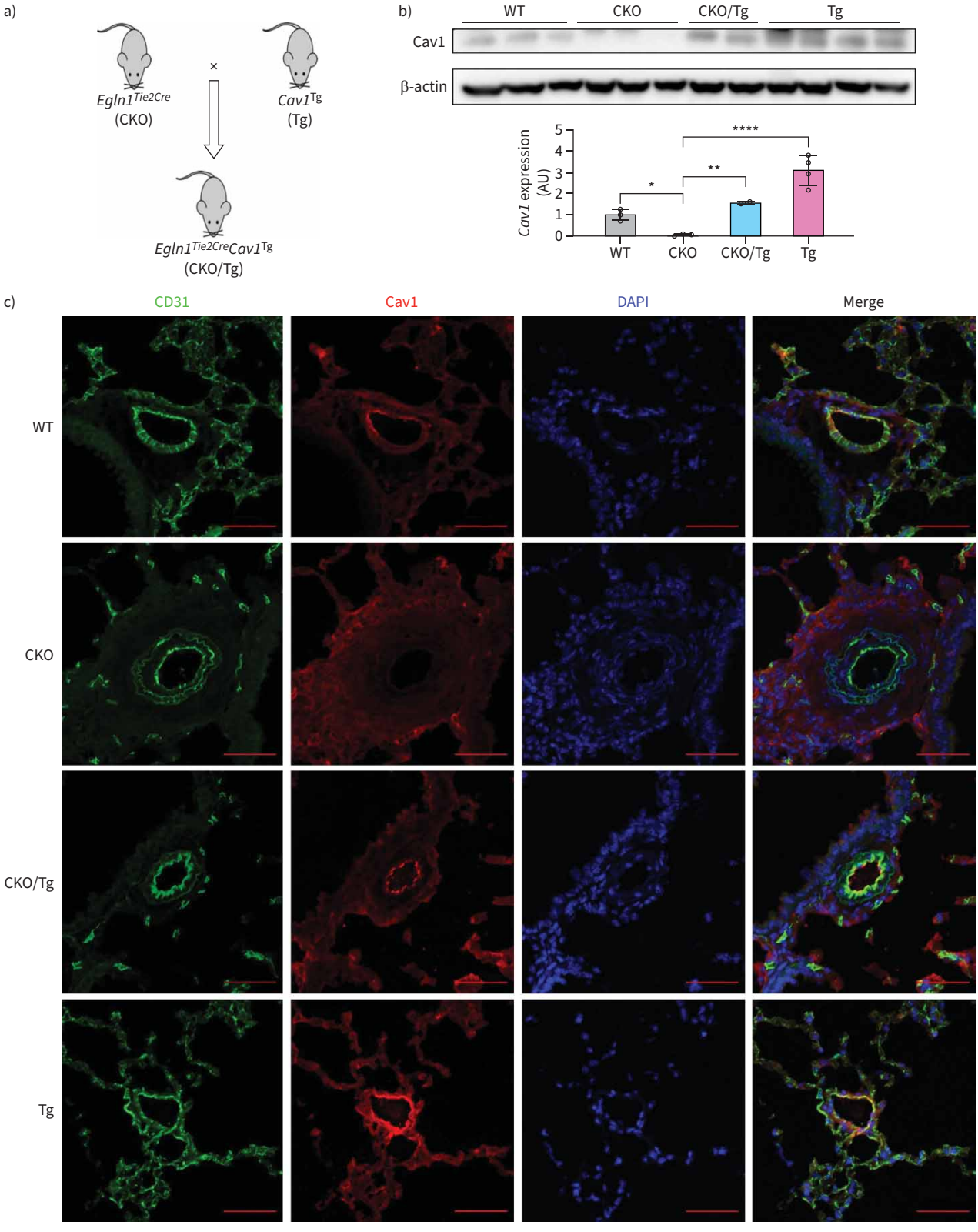

FIGURE 5 Caveolin 1 (Cav1) transgenic expression in *Egln1*^{Tie2Cre} (CKO) mice. a) Strategy of generating *Egln1*^{Tie2Cre}/*Cav1*^{Tg} (CKO/Tg) mice by breeding Cav1 transgenic mice (*Cav1*^{Tg}) into the genetic background of CKO mice. b) Western blotting demonstrating restored Cav1 expression in CKO/Tg mouse lungs. c) Immunostaining demonstrated that Cav1 expression was downregulated in lung endothelial cells of CKO mice compared to wild type (WT) and restored in CKO/Tg mice. Lung sections were immunostained with anti-Cav1 (red) and CD31 (green). Nuclei were counterstained with DAPI (blue). Scale bars: 50 μm. Statistical significance for b determined by one-way ANOVA with Tukey *post hoc* analysis. *: p<0.05; **: p<0.01; ****: p<0.0001.

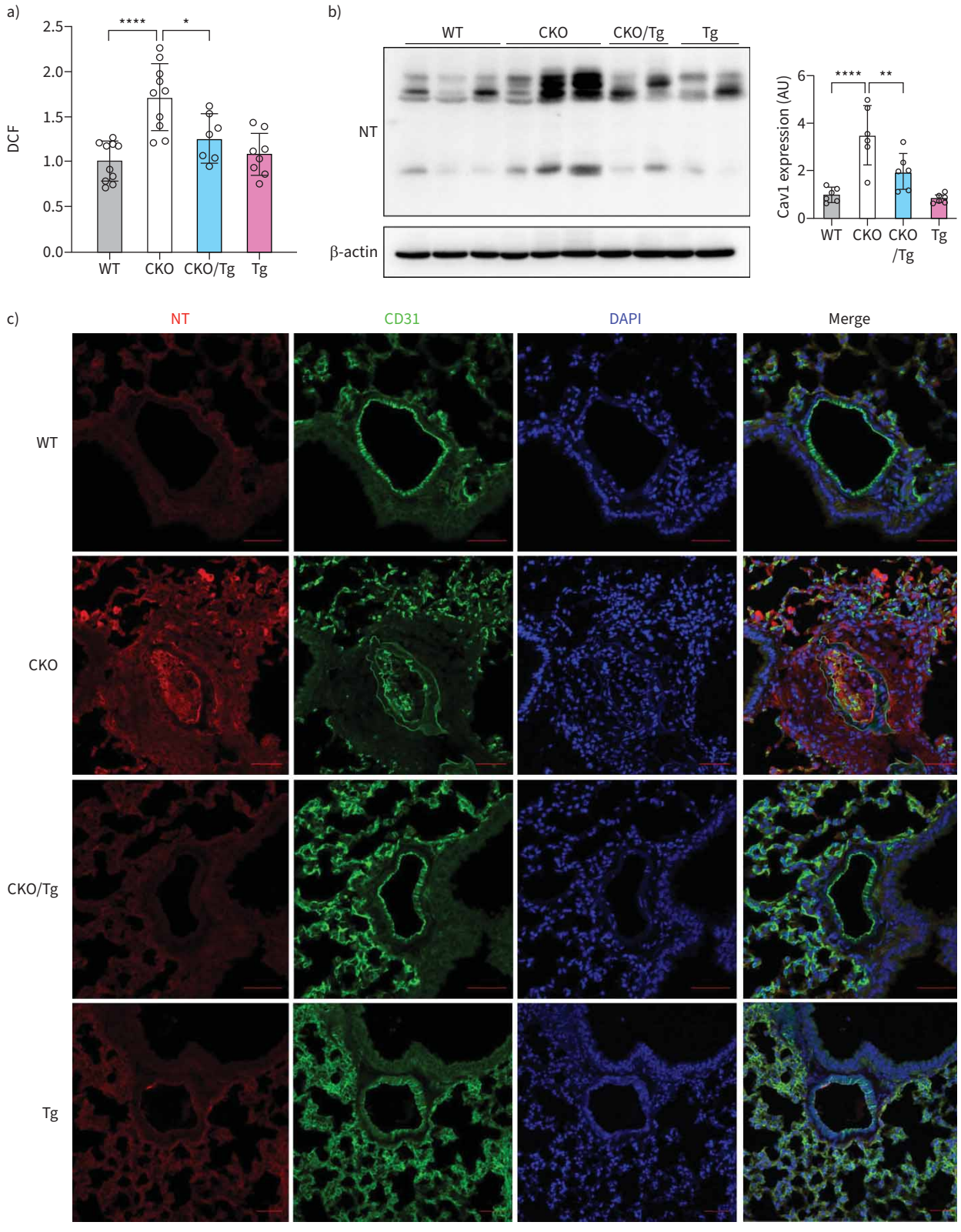

FIGURE 6 Caveolin 1 (Cav1) transgenic expression inhibited excessive reactive oxygen species (ROS)/reactive nitrogen species (RNS) in *Egln1*^{Tie2Cre} (CKO) mouse lungs. a) 2′, 7′-dichlorodihydrofluorescein (DCF) measurements demonstrating that the increased production of ROS/RNS seen in CKO mouse lungs was inhibited in *Egln1*^{Tie2Cre}/*Cav1*^{Tg} (CKO/Tg) mouse lungs. There was no marked difference in lung generation of ROS/RNS in *Egln1*$^{f/f}$/*Cav1*^{Tg} (Tg) mice compared to wild type (WT) mice. WT and CKO data shared with figure 1a. b) Western blotting demonstrated a reduction in nitrotyrosine (NT) levels in CKO/Tg mice compared to CKO mice. c) Representative immunostaining showed that CKO/Tg mice exhibited reduced

NT levels compared to CKO mice. Lung sections were immunostained with anti-NT (red) and CD31 (green). Nuclei were counterstained with DAPI (blue). Scale bars: 50 μm. Statistical significance in a and b determined by one-way ANOVA with Tukey's *post hoc* analysis. *: p<0.05; **: p<0.01; ****: p<0.0001.

critical for the maintenance of vascular homeostasis in this severe PH model. *Nos3* (encoding eNOS) but neither *Nos1* nor *Nos2* was upregulated in the CKO lungs (figure 3a and supplementary figure S3), and *Nos3* normalised in lungs of *Egln1* and *Hif2a* double knockout mice ($Egln1^{Tie2Cre}/Hif2a^{Tie2Cre}$ (EH2)), suggesting that eNOS mediates nitrative stress in CKO mice. To investigate this, we leveraged nanoparticle delivery of CRISPR–Cas9 plasmid DNA [27] expressing Cas9 under the control of the *CDH5* promoter and *Nos3*-specific gRNAs driven by the *U6* promoter to specifically knockdown *Nos3* in ECs of CKO mice (figure 3b). We observed ∼30% genome editing efficiency in lung ECs of *Nos3* gRNA plasmid DNA-treated CKO mice (supplementary figure S4), and diminished eNOS protein expression (figure 3c). Immunostaining also showed diminished eNOS expression in lung ECs of these mice compared with control mice (figure 3d), demonstrating successful knockdown of *Nos3* in CKO lung ECs. Accordingly, NT levels were also markedly decreased in lung ECs of these *Nos3* gRNA plasmid DNA-treated CKO mice (figure 3c, e). Haemodynamic measurements showed that *Nos3* knockdown in ECs significantly reduced RVSP and RV/(LV+S) ratio in these CKO mice (figure 3f, g). Pulmonary vascular remodelling, assessed *via* PA wall thickness (figure 3h, i), and muscularisation of distal pulmonary vessels (figure 3j, k) were also markedly attenuated in these mice. Additionally, all five *Nos3* gRNA plasmid DNA-treated mice survived, compared to 50% mortality in control CKO mice during the same period. These data demonstrate that eNOS is the primary source of nitrative stress, which contributes to the development of occlusive remodelling and severe PH seen in CKO mice.

Decreased expression of endothelial Cav1 secondary to PHD2 deficiency in a HIF-2α-dependent manner

Cav1 deficiency activates eNOS and increases ROS/RNS production, leading to nitrative stress, which post-translationally modifies PKG through tyrosine nitration and impairs its kinase activity, leading to PH [16, 19]. To find out whether dysregulation of Cav1 signalling is involved in the generation of nitrative stress and PH development in CKO mice, we first checked the expression level of Cav1 in the lungs of CKO mice. As shown in figure 4a, *Cav1* mRNA levels were markedly decreased in the lungs of CKO mice compared to those in similar age WT mice. HIF-2α deletion in CKO (EH2) mice restored *Cav1* mRNA expression (figure 4a). Western blotting also demonstrated reduced Cav1 protein levels in CKO lungs, which was reversed in EH2 mice and in fact increased in EH2 mouse lungs compared to WT lungs (figure 4b, c). By performing immunofluorescent staining, we found that Cav1 is co-stained with $CD31^+$ cells (*i.e.* ECs) in the pulmonary vasculature of WT mice whereas it is diminished in pulmonary vascular lesions in CKO mice and restored in pulmonary vascular ECs of EH2 mice (figure 4d), suggesting that endothelial Cav1 is reduced by PHD2 deficiency dependent on HIF-2α activation in $Egln1^{Tie2Cre}$ mice.

Restored Cav1 expression inhibited nitrative stress in $Egln1^{Tie2Cre}/Cav1^{Tg}$ *mice*

To determine whether Cav1 deficiency is responsible for the augmentation of nitrative stress *via* eNOS activation and the pathogenesis of PH in CKO mice, we generated a mouse model with Cav1 transgenic expression under control of the preproET-1 promoter in the genetic background of CKO mice ($Egln1^{Tie2Cre}/Cav1^{Tg}$ (CKO/Tg)) (figure 5a) [23]. Western blotting and immunostaining demonstrated that reduced Cav1 expression seen in CKO mouse lungs was restored in CKO/Tg mice (figure 5b, c). Restored Cav1 expression in CKO mice drastically reduced the levels of ROS/RNS in the lungs of CKO/Tg mice compared to CKO mice (figure 6a). Further examination of NT levels *via* Western blotting and immunostaining showed that NT levels were inhibited in the lung and pulmonary vascular ECs of CKO/Tg mice compared to CKO mice (figure 6b, c), suggesting that Cav1 deficiency is responsible for the increased oxidative/nitrative stress in CKO mouse lungs.

Cav1 transgenic expression attenuates PH seen in $Egln1^{Tie2Cre}$ *mice*

We next determined if Cav1 transgenic expression in CKO mice would rescue the hypertensive pulmonary phenotype. Haemodynamic measurement demonstrated a partial decrease of RVSP in CKO/Tg at age 3.5 months compared to CKO mice (figure 7a). RV hypertrophy was also attenuated in CKO/Tg mice (figure 7b). Pathological examination showed that CKO/Tg mice had reduced pulmonary vascular remodelling, including decreases in neointima and occlusive lesions (figure 7c), PA wall thickness (figure 7d) and muscularisation of distal pulmonary vessels in comparison to CKO mice (figure 7e, f).

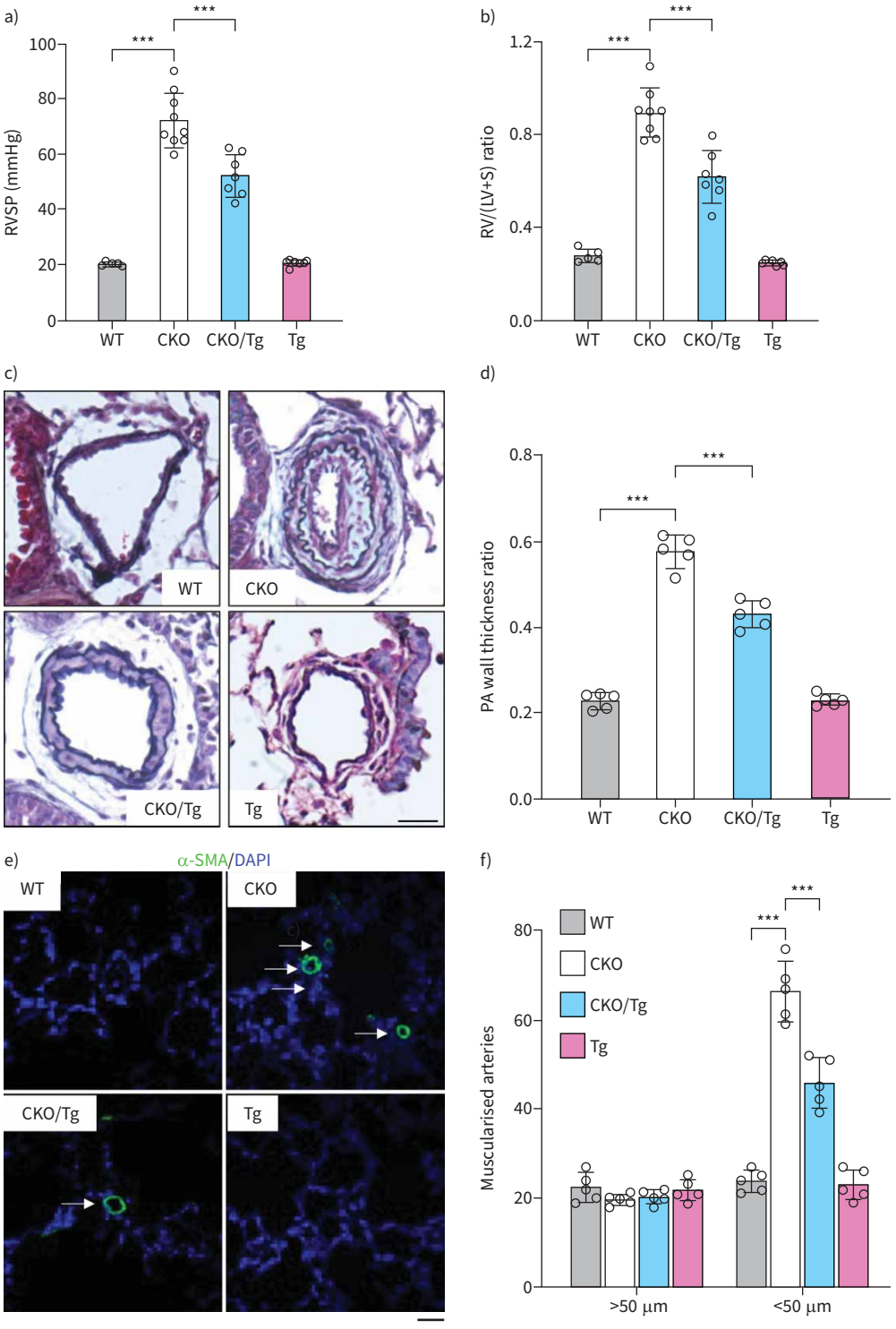

FIGURE 7 Transgenic expression of caveolin 1 (Cav1) inhibited severe pulmonary hypertension seen in *Egln1*^{Tie2Cre} (CKO) mice. a, b) *Egln1*^{Tie2Cre}/*Cav1*^{Tg} (CKO/Tg) mice exhibited marked decreases of right ventricular systolic pressure (RVSP) (a) and right ventricular hypertrophy (weight ratio of right ventricle/left ventricle plus septum (RV/(LV+S)) (b) compared to CKO mice at age 3.5 months. c, d) Representative micrographs of Russell–Movat pentachrome staining showing inhibited obliterative vascular remodelling including diminished neointima formation and reduced pulmonary artery (PA) wall thickness in the lung of CKO/Tg mice. Scale bar: 50 μm. e, f) Immunostaining of α-smooth muscle actin (α-SMA) demonstrating inhibition of muscularisation of distal pulmonary vessels in the lungs of CKO/Tg mice. Arrows indicate muscularised pulmonary vessels. Statistical significance in a, b, d and f determined by one-way ANOVA with Tukey's *post hoc* analysis. ***: p<0.001.

Cav1 transgenic expression normalises RV and PA functions in Egln1^{Tie2Cre}/Cav1^{Tg} *mice*

We next evaluated whether Cav1 transgenic expression inhibits the right heart dysfunction seen in CKO mice. Echocardiography showed that CKO/Tg mice had marked decreases of RV wall thickness compared to CKO mice (figure 8a–c). CKO/Tg mice also exhibited marked improvements of RV contractility assessed by RV fraction area change (figure 8d, and supplementary videos S1 and S2). However, we did not observe a significant change in heart rate, cardiac output or LV fractional shortening in CKO/Tg mice compared with CKO mice (supplementary figure S5a–c). CKO/Tg mice exhibited improved PA function, assessed by PA acceleration time/ejection time ratio, compared to CKO mice (figure 8e). These data demonstrate that Cav1 transgenic expression partially but significantly rescues the defective PA and RV functions seen in CKO mice.

Discussion

The present study demonstrated that nitrative stress was markedly augmented in the lungs, especially in vascular lesions of CKO mice, recapitulating the pathological feature of clinical PAH. Augmentation of nitrative stress was due to endothelial Cav1 deficiency and eNOS activation. Cav1 transgenic expression in CKO/Tg mice reduced nitrative stress levels and attenuated PH, evidenced by a reduction in RVSP, pulmonary vascular remodelling and RV hypertrophy, as well as improvements in RV and PA function. Both pharmacological scavenging of ROS/RNS and genetic knockdown of endothelial Nos3 *via* EC-targeted nanoparticle delivery of CRISPR–Cas9 technology in adult mice diminished nitrative stress and markedly reduced the severity of pulmonary vascular remodelling and PH in CKO mice. These findings suggest that restoration of Cav1 expression and ROS/RNS scavenging represent potential therapeutic strategies for the treatment of severe PAH, including IPAH (figure 8f). The clinical relevance is validated by our previous observation that PHD2 expression was diminished in ECs of occlusive pulmonary vessels in IPAH patients [20].

Prominent oxidative/nitrative stress is a pathological feature of clinical PAH [10, 15, 16]. Our recent study showed for the first time that CKO mice spontaneously develop severe PH with obliterative pulmonary vascular remodelling, including occlusive vascular lesions, formation of plexiform-like lesions and marked elevation of RVSP ranging from 70–100 mmHg as well as development of right heart failure [20]. Here we show a marked increase of ROS/RNS in CKO mouse lungs and prominent anti-NT staining indicative of extensive nitrative stress in pulmonary vascular lesions, especially in ECs and inflammatory cells. This study provides further evidence that CKO mice are an excellent mouse model of human PAH. Furthermore, treatment of the mice with the ROS scavenger MnTMPyP inhibited occlusive pulmonary vascular remodelling and attenuated PH, demonstrating the pathogenic role of oxidative/nitrative stress in the severity of PH.

Nitrative stress is created by excessive superoxide and NO, which chemically react to form peroxynitrite. We found that expression of *Nos3* but neither *Nos1* nor *Nos2* was markedly increased in CKO lungs. To specifically inhibit peroxynitrite formation, we employed the EC-targeted nanoparticle delivery of CRISPR plasmid DNA technology to selectively disrupt *Nos3* expression in ECs in adult CKO mice, which resulted in diminished nitrative stress in CKO lungs and especially in pulmonary vascular ECs. These data demonstrate that ECs are the primary sources of nitrative stress *via* eNOS expression and activation secondary to PHD2 deficiency in CKO lungs. Given that peroxynitrite is more stable and diffusible than NO, EC-derived nitrative stress can easily spread into other cell types in the lesions, such as pulmonary vascular SMCs, fibroblasts and infiltrated proinflammatory cells. Thus, EC-specific *Nos3* knockdown results in decreased nitrative stress not only in ECs but also in whole lungs. Additionally, EC-derived peroxynitrite diffuses to pulmonary vascular SMCs and induces tyrosine nitration of PKG expressed in SMCs, which impairs its kinase activity, leading to pulmonary vascular remodelling and PH development. Consistently, we observed reduced RVSP, pulmonary vascular remodelling and RV hypotrophy in endothelial *Nos3*-disrupted CKO mice. Together, these data provide unequivocal evidence of nitrative stress derived from endothelial dysfunction contributing to obliterative pulmonary vascular remodelling and severe PH development.

Previous studies have shown decreases of *CAV1* mRNA and protein levels in lung ECs of patients with PAH [16]. Cav1 deficiency is also evident in the arterial lesions of PH rats, including both the Sugen5416/hypoxia-induced PH and monocrotaline-induced PH models [29, 30]. Our previous study provides the first genetic evidence that Cav1 deficiency induces PH in mice [17]. A recent study showed that Cav1 deficiency in ECs promotes more severe PH in response to hypoxia [31]. Consistently, *CAV1* mutation is associated with heritable PAH in patients [32]. Together, these studies provide clear evidence of CAV1 deficiency in the pathogenesis of PH. Our other study has shown that genetic deletions of both *Cav1* and *Nos3* or treatment of *Cav1*$^{-/-}$ mice with either NO synthase inhibitor L-NAME or ROS/RNS scavenger

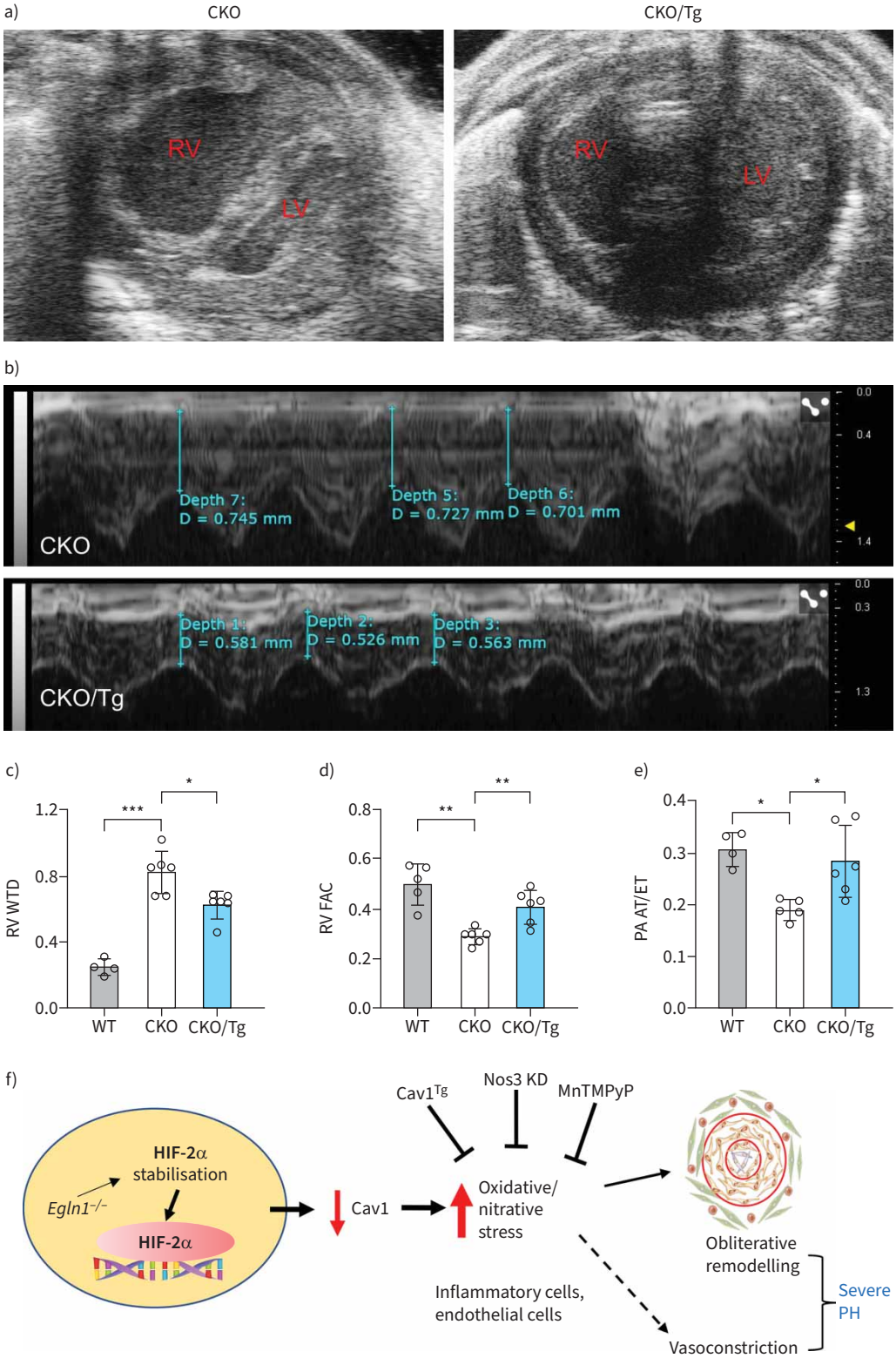

FIGURE 8 Caveolin 1 (Cav1) transgenic expression improved right heart and pulmonary artery (PA) functions in *Egln1*^{Tie2Cre}/*Cav1*^{Tg} (CKO/TG) mice. a) Representative echocardiography B-mode showing reduced right ventricle (RV) chamber size in CKO/Tg mice compared to *Egln1*^{Tie2Cre} (CKO) mice. b) Representative echocardiography M-mode showing reduced RV wall thickness at diastolic stage in CKO/Tg mice compared to CKO mice. c) RV wall thickening seen in CKO mice was reduced in CKO/Tg mice. d) RV contractility as determined by fraction area change (FAC) was improved by restored endothelial Cav1 expression in CKO/Tg mice compared to CKO

mice. e) PA function assessed by PA acceleration time/ejection time (AT/ET) ratio was rescued in CKO/Tg mice. f) Endothelial prolyl hydroxylase 2 (PHD2) deficiency induces decreases in endothelial Cav1 expression and endothelial nitric oxide synthase (eNOS) activation resulting in augmented nitrative stress, which contributes to obliterative pulmonary vascular remodelling and severe pulmonary hypertension (PH). Restoration of endothelial Cav1 expression or reactive oxygen species/reactive nitrogen species scavenging could be effective therapeutic approaches for the treatment of pulmonary arterial hypertension. Statistical significance in c–e determined by one-way ANOVA with Tukey's *post hoc* analysis. LV: left ventricle; WTD: wall thickness during diastole; HIF-2α: hypoxia-inducible factor-2α; KD: knockdown; MnTMPyP: manganese (III) tetrakis (1-methyl-4-pyridyl) porphyrin pentachloride. *: p<0.05; **: p<0.01; ***: p<0.001.

MnTMPyP inhibited the PH seen in *Cav1*$^{-/-}$ mice, suggesting that chronic activation of eNOS secondary to Cav1 deficiency is the mechanism of PH induced by CAV1 deficiency [16]. Others have also shown that L-NAME treatment inhibits PH in *Cav1*$^{-/-}$ mice [33]. It has been shown that eNOS activation secondary to Cav1 deficiency leads to peroxynitrite formation, which causes PKG nitration in *Cav1*$^{-/-}$ mice. PKG nitration impairs its kinase activity and thereby induces pulmonary vascular remodelling and PH [16]. eNOS activation and PKG nitration is prominent in lung tissues of IPAH patients [16, 34]. These studies provide unequivocal evidence that Cav1 deficiency induces nitrative stress, leading to PKG nitration and thus PH.

In CKO mice, we observed elevated levels of ROS/RNS and PKG nitration and decreased endothelial Cav1 expression. We demonstrated that Cav1 deficiency in CKO mice is involved in the regulation of nitrative stress because Cav1 transgenic expression normalises the levels of ROS/RNS and inhibits nitrative stress, as evidenced by diminished NT levels in pulmonary vascular ECs, and thus inhibits obliterative pulmonary vascular remodelling and reduces PH as well as improves RV and PA function in CKO mice. We observed complete inhibition of occlusive vascular remodelling without neointima formation in CKO/Tg mice, endothelial *Nos3* knockdown CKO mice and MnTMPyP-treated CKO mice. The medial thickness was less affected in these mice, which is consistent with the markedly reduced but still elevated RVSP. Together, our data demonstrate that endothelial Cav1 deficiency secondary to PHD2 deficiency mediates the augmentation of nitrative stress in CKO mouse lungs *via* activation of endothelial Nos3, which leads to obliterative pulmonary vascular lesions and severe PH.

The current studies demonstrate that treatment with the ROS/RNS scavenger MnTMPyP attenuates both RVSP and vascular remodelling in CKO mice, which is consistent with a previous observation that antioxidant N-acetylcysteine treatment reduces PH induced by chronic hypoxia in rats [35]. However, another antioxidant, TEMPOL, has a beneficial effect on reducing RVSP but not arterial remodelling in the hypoxia and SU5416/hypoxia-induced PH rat model [36]. Thus, whether antioxidant therapies are effective in preclinical models of PH is still controversial, but this controversy might be due to the selected agents, doses and design of experiments [37]. For example, depending on the concentration and lung cell types, TEMPOL can be pro-oxidant or antioxidant [38]. Other studies also show that high concentrations of or extended exposure to TEMPOL increases ROS levels [39, 40]. Further studies are warranted to address this important question of whether antioxidants should be given to PAH patients for treatment of the disease.

In summary, we have demonstrated prominent nitrative stress in vascular lesions of CKO mice, which is mediated by endothelial Cav1 deficiency ascribed to HIF-2α activation and resultant eNOS activation. ROS/RNS scavenger treatment, CRISPR-mediated endothelial *Nos3* knockdown or transgenic expression of Cav1 inhibit nitrative stress and obliterative pulmonary vascular remodelling and attenuate PH in CKO mice. Thus, Cav1 deficiency-induced oxidative/nitrative stress secondary to PHD2 deficiency is a part of the mechanism of severe PH in CKO mice, as seen in PAH patients.

Acknowledgement: We greatly appreciate William C. Sessa from the Departments of Pharmacology and Medicine at Yale School of Medicine for his generosity in providing us with the *Cav1*^{Tg} mice.

Author contributions: Z. Dai and Y-Y. Zhao conceived the experiments. Z. Dai, B. Liu, D. Yi, J. Dai, N. Machireddy, D. Dong, K. Ramirez, Y. Peng and M.M. Zhu designed and carried out experiments, and analysed the data. Z. Dai, R. Vanderpool and Y-Y. Zhao analysed and interpreted the data. Z. Dai wrote the manuscript. Z. Dai and Y-Y. Zhao supervised the project and revised the manuscript. All authors approved the manuscript.

Conflict of interest: Y-Y. Zhao is the founder and chief scientific officer of MountView Therapeutics LLC. This project utilises technologies subject to the following pending patents entitled "PLGA-PEG nanoparticles and

methods of uses" and "Cationic polymer-formulated nanoparticles and methods of use" to Y-Y. Zhao. The other authors declare no conflicts of interest.

Support statement: This work was supported in part by National Institutes of Health (NIH) (grants R01HL133951, R01HL140409, R01HL148810 and R01HL164014) to Y-Y. Zhao, and by NIH (R00HL13827 and R01HL158596), AHA Career Development Award (20CDA35310084), ATS Foundation Pulmonary Hypertension Association Research Fellowship, Arizona Biomedical Research Cente (ADHS18-198871) and the University of Arizona departmental start-up funding to Z. Dai. Funding information for this article has been deposited with the Crossref Funder Registry.

Reference

1 McLaughlin VV, Archer SL, Badesch DB, *et al.* ACCF/AHA 2009 expert consensus document on pulmonary hypertension. *Circulation* 2009; 119: 2250–2294.
2 Hoeper MM, Bogaard HJ, Condliffe R, *et al.* Definitions and diagnosis of pulmonary hypertension. *J Am Coll Cardiol* 2013; 62: D42–D50.
3 Hautefort A, Mendes-Ferreira P, Sabourin J, *et al.* Bmpr2 mutant rats develop pulmonary and cardiac characteristics of pulmonary arterial hypertension. *Circulation* 2019; 139: 932–948.
4 Stacher E, Graham BB, Hunt JM, *et al.* Modern age pathology of pulmonary arterial hypertension. *Am J Respir Crit Care Med* 2012; 186: 261–272.
5 Sutendra G, Michelakis ED. Pulmonary arterial hypertension: challenges in translational research and a vision for change. *Sci Transl Med* 2013; 5: 208sr5.
6 McLaughlin VV, Shah SJ, Souza R, *et al.* Management of pulmonary arterial hypertension. *J Am Coll Cardiol* 2015; 65: 1976–1997.
7 Pullamsetti SS, Schermuly R, Ghofrani A, *et al.* Novel and emerging therapies for pulmonary hypertension. *Am J Respir Crit Care Med* 2014; 189: 394–400.
8 Spiekermann S, Schenk K, Hoeper MM. Increased xanthine oxidase activity in idiopathic pulmonary arterial hypertension. *Eur Respir J* 2009; 34: 276.
9 Jankov RP, Kantores C, Pan J, *et al.* Contribution of xanthine oxidase-derived superoxide to chronic hypoxic pulmonary hypertension in neonatal rats. *Am J Physiol Cell Mol Physiol* 2008; 294: L233–L245.
10 Evans CE, Zhao Y-Y. Molecular basis of nitrative stress in the pathogenesis of pulmonary hypertension. *Adv Exp Med Biol* 2017; 967: 33–45.
11 Bowers R, Cool C, Murphy RC, *et al.* Oxidative stress in severe pulmonary hypertension. *Am J Respir Crit Care Med* 2004; 169: 764–769.
12 Masri FA, Comhair SAA, Dostanic-Larson I, *et al.* Deficiency of lung antioxidants in idiopathic pulmonary arterial hypertension. *Clin Transl Sci* 2008; 1: 99–106.
13 Beckman JS, Beckman TW, Chen J, *et al.* Apparent hydroxyl radical production by peroxynitrite: implications for endothelial injury from nitric oxide and superoxide. *Proc Natl Acad Sci USA* 1990; 87: 1620–1624.
14 Beckman JS, Koppenol WH. Nitric oxide, superoxide, and peroxynitrite: the good, the bad, and ugly. *Am J Physiol* 1996; 271: C1424–C1437.
15 Fulton D, Li X, Bordan Z, *et al.* Reactive oxygen and nitrogen species in the development of pulmonary hypertension. *Antioxidants* 2017; 6: 54.
16 Zhao Y-Y, Zhao YD, Mirza MK, *et al.* Persistent eNOS activation secondary to caveolin-1 deficiency induces pulmonary hypertension in mice and humans through PKG nitration. *J Clin Invest* 2009; 119: 2009–2018.
17 Zhao Y-Y, Liu Y, Stan R-V, *et al.* Defects in caveolin-1 cause dilated cardiomyopathy and pulmonary hypertension in knockout mice. *Proc Natl Acad Sci USA* 2002; 99: 11375–11380.
18 Zhao YD, Cai L, Mirza MK, *et al.* Protein kinase G-I deficiency induces pulmonary hypertension through Rho A/Rho kinase activation. *Am J Pathol* 2012; 180: 2268–2275.
19 Zhao Y-Y, Malik AB. A novel insight into the mechanism of pulmonary hypertension involving caveolin-1 deficiency and endothelial nitric oxide synthase activation. *Trends Cardiovasc Med* 2009; 19: 238–242.
20 Dai Z, Li M, Wharton J, *et al.* Prolyl-4 hydroxylase 2 (PHD2) deficiency in endothelial cells and hematopoietic cells induces obliterative vascular remodeling and severe pulmonary arterial hypertension in mice and humans through hypoxia-inducible factor-2α. *Circulation* 2016; 133: 2447–2458.
21 Dai Z, Zhao Y-Y. Discovery of a murine model of clinical PAH: mission impossible? *Trends Cardiovasc Med* 2017; 27: 229–236.
22 Bauer PM, Yu J, Chen Y, *et al.* Endothelial-specific expression of caveolin-1 impairs microvascular permeability and angiogenesis. *Proc Natl Acad Sci USA* 2005; 102: 204–209.
23 Murata T, Lin MI, Huang Y, *et al.* Reexpression of caveolin-1 in endothelium rescues the vascular, cardiac, and pulmonary defects in global caveolin-1 knockout mice. *J Exp Med* 2007; 204: 2373–2382.
24 Yi D, Liu B, Wang T, *et al.* Endothelial autocrine signaling through cxcl12/cxcr4/foxm1 axis contributes to severe pulmonary arterial hypertension. *Int J Mol Sci* 2021; 22: 3182.

25 Dai Z, Zhu MM, Peng Y, *et al.* Therapeutic targeting of vascular remodeling and right heart failure in pulmonary arterial hypertension with a HIF-2α inhibitor. *Am J Respir Crit Care Med* 2018; 198: 1423–1434.

26 Dai Z, Zhu MM, Peng Y, *et al.* Endothelial and smooth muscle cell interaction via FoxM1 signaling mediates vascular remodeling and pulmonary hypertension. *Am J Respir Crit Care Med* 2018; 198: 788–802.

27 Zhang X, Jin H, Huang X, *et al.* Robust genome editing in adult vascular endothelium by nanoparticle delivery of CRISPR-Cas9 plasmid DNA. *Cell Rep* 2022; 38: 110196.

28 Peng YJ, Yuan G, Ramakrishnan D, *et al.* Heterozygous HIF-1α deficiency impairs carotid body-mediated systemic responses and reactive oxygen species generation in mice exposed to intermittent hypoxia. *J Physiol* 2006; 577: 705–716.

29 Achcar ROD, Demura Y, Rai PR, *et al.* Loss of caveolin and heme oxygenase expression in severe pulmonary hypertension. *Chest* 2006; 129: 696–705.

30 Mathew R, Huang J, Shah M, *et al.* Disruption of endothelial-cell caveolin-1α/raft scaffolding during development of monocrotaline-induced pulmonary hypertension. *Circulation* 2004; 110: 1499–1506.

31 Oliveira SDS, Chen J, Castellon M, *et al.* Injury-induced shedding of extracellular vesicles depletes endothelial cells of Cav-1 (caveolin-1) and enables TGF-β (transforming growth factor-β)–dependent pulmonary arterial hypertension. *Arterioscler Thromb Vasc Biol* 2019; 39: 1191–1202.

32 Austin ED, Ma L, LeDuc C, *et al.* Whole exome sequencing to identify a novel gene (caveolin-1) associated with human pulmonary arterial hypertension. *Circ Cardiovasc Genet* 2012; 5: 336–343.

33 Wunderlich C, Schmeisser A, Heerwagen C, *et al.* Chronic NOS inhibition prevents adverse lung remodeling and pulmonary arterial hypertension in caveolin-1 knockout mice. *Pulm Pharmacol Ther* 2008; 21: 507–515.

34 Aggarwal S, Gross CM, Rafikov R, *et al.* Nitration of tyrosine 247 inhibits protein kinase G-1α activity by attenuating cyclic guanosine monophosphate binding. *J Biol Chem* 2014; 289: 7948–7961.

35 Hoshikawa Y, Ono S, Suzuki S, *et al.* Generation of oxidative stress contributes to the development of pulmonary hypertension induced by hypoxia. *J Appl Physiol (1985)* 2001; 90: 1299–1306.

36 Voelkel NF, Bogaard HJ, Al HA, *et al.* Antioxidants for the treatment of patients with severe angioproliferative pulmonary hypertension? *Antioxidants Redox Signal* 2013; 18: 1810–1817.

37 Suzuki YJ, Steinhorn RH, Gladwin MT. Antioxidant therapy for the treatment of pulmonary hypertension. *Antioxidants Redox Signal* 2013; 18: 1723–1726.

38 Park WH. TEMPOL differently affects cellular redox changes and antioxidant enzymes in various lung-related cells. *Sci Rep* 2021; 11: 14869.

39 Han YH, Park WH. TEMPOL inhibits growth of As4.1 juxtaglomerular cells via cell cycle arrest and apoptosis. *Oncol Rep* 2012; 27: 842–848.

40 Wang M, Li K, Zou Z, *et al.* Piperidine nitroxide tempol enhances cisplatin-induced apoptosis in ovarian cancer cells. *Oncol Lett* 2018; 16: 4847–4854.